

The role of propeptide-mediated autoinhibition and intermolecular chaperone in the maturation of cognate catalytic domain in leucine aminopeptidase

Article

Accepted Version

Creative Commons: Attribution-Noncommercial-No Derivative Works 4.0

Baltulionis, G., Blight, M., Robin, A., Charalampopoulos, D. ORCID: <https://orcid.org/0000-0003-1269-8402> and Watson, K. A. ORCID: <https://orcid.org/0000-0002-9987-8539> (2021) The role of propeptide-mediated autoinhibition and intermolecular chaperone in the maturation of cognate catalytic domain in leucine aminopeptidase. *Journal of Structural Biology*, 213 (3). 107741. ISSN 1047-8477 doi: <https://doi.org/10.1016/j.jsb.2021.107741> Available at <https://centaur.reading.ac.uk/98601/>

It is advisable to refer to the publisher's version if you intend to cite from the work. See [Guidance on citing](#).

To link to this article DOI: <http://dx.doi.org/10.1016/j.jsb.2021.107741>

Publisher: Elsevier

including copyright law. Copyright and IPR is retained by the creators or other copyright holders. Terms and conditions for use of this material are defined in the [End User Agreement](#).

www.reading.ac.uk/centaur

CentAUR

Central Archive at the University of Reading

Reading's research outputs online

1 **The role of propeptide-mediated autoinhibition and**
2 **intermolecular chaperone in the maturation of**
3 **cognate catalytic domain in leucine aminopeptidase**

4
5 G. Baltulionis^{1,2}, M. Blight³, A. Robin³, D. Charalampopoulos², K.A. Watson^{1*}

6 School of Biological Sciences¹ and Department of Food and Nutritional Sciences²,
7 Whiteknights Campus, University of Reading, Reading, UK, RG6 6AS; Biocatalysts
8 Limited³, Cefn Coed Parc Nantgarw, Wales, UK, CF15 7QQ.

9

10 *Corresponding author

11

12

13

14

15

16

17

18

19

20 **Abstract**

21 Leucyl aminopeptidase A from *Aspergillus oryzae* RIB40 (AO-LapA) is an exo-acting
22 peptidase, widely utilised in food debittering applications. AO-LapA is secreted as a
23 zymogen by the host and requires enzymatic cleavage of the autoinhibitory propeptide to
24 reveal its full activity. Scarcity of structural data of zymogen aminopeptidases hampers a
25 better understanding of the details of their molecular action of autoinhibition and how this
26 might be utilised to improve the properties of such enzymes by recombinant methods for
27 more effective bioprocessing. To address this gap in the literature, herein we report high-
28 resolution crystal structures of recombinantly expressed AO-LapA precursor (AO-*pro*LapA),
29 mature LapA (AO-*m*LapA) and AO-*m*LapA complexed with reaction product l-leucine (AO-
30 *m*LapA-Leu), all purified from *Pichia pastoris* culture supernatant. Our structures reveal a
31 plausible molecular mechanism of LapA catalytic domain autoinhibition by propeptide and
32 highlights the role of intramolecular chaperone (IMC). Our data suggest an absolute
33 requirement for IMC in the maturation of cognate catalytic domain of AO-LapA. This
34 observation is reinforced by our expression and refolding data of catalytic domain only (AO-
35 *ref*LapA) from *Escherichia coli* inclusion bodies, revealing a limited active conformation.
36 Our work supports the notion that known synthetic aminopeptidase inhibitors and substrates
37 mimic key polar contacts between propeptide and corresponding catalytic domain,
38 demonstrated in our AO-*pro*LapA zymogen crystal structure. Furthermore, understanding the
39 atomic details of the autoinhibitory mechanism of cognate catalytic domains by native
40 propeptides has wider reaching implications toward synthetic production of more effective
41 inhibitors of bimetallic aminopeptidases and other dizinc enzymes that share an analogous
42 reaction mechanism.

43 **Keywords:** leucine aminopeptidase, propeptide, autoinhibition, refolding, zymogen

44 **Introduction**

45 Aminopeptidases are utilised in the food industry for sensory applications and development
46 of food flavour profile. Aminopeptidases are indispensable in protein hydrolysate debittering,
47 since they remove hydrophobic amino acids from the N-terminus of peptide hydrolysates,
48 which contribute to bitterness of the flavour profile [1-3]. Fungal aminopeptidases from
49 *Aspergillus oryzae* are generally recognized as safe (GRAS) by the food industry, with a long
50 history of utilisation in debittering applications. Efforts to characterise their role in this
51 process, led to earlier work to over-express and biochemically characterize the extracellular
52 leucine aminopeptidase A from *A. oryzae* RIB40 (AO-LapA) [4]. To date, no additional
53 reports of exogenous over-expression of this high-utility aminopeptidase exist in the
54 literature. Also lacking are attempts of successful production of such peptidases in *Pichia*
55 *pastoris*, an important GRAS organism used in the food industry.

56 To our knowledge, there have been no published data for the crystal structures of the leucine
57 aminopeptidases used in the food industry. The scarcity of precise structural data for these
58 predominantly fungal peptidases inhibits our understanding of their reaction-inhibition
59 mechanisms and substrate specificities. For example, there are only 12 amino acid differences
60 between the full sequences of AO-LapA and AS-Lap1 (leucine aminopeptidase from
61 *Aspergillus sojae*), which mostly occur outside the active site pocket, that is responsible for
62 their quite distinct substrate preferences [5].

63 It is well established, that pro-domains of secretory endo- and exopeptidases play an
64 important role in the inhibition of their cognate catalytic domains, which undergo activation
65 by removal of the pro-domain either by autocatalytic processing or external endopeptidase
66 activity. By secreting protease precursors in a zymogen form, undesirable cytosolic activation
67 and proteolysis events are prevented [6]. Typically, the zymogen conversion does not involve
68 conformational changes of catalytic residues and the active sites are sterically rendered

69 inaccessible to substrate by the unique residues of pro-domain or prosegment, thus preventing
70 activity [7]. In addition, N-terminal propeptides are known to act as intramolecular
71 chaperones (IMC), decreasing the energy barrier of transition from a molten globule
72 intermediate to a kinetically trapped native state [8]. In this respect, a well-studied model
73 enzyme, subtilisin, has been shown to be unable to escape the folding transition state
74 between a molten-globule and a native conformation, without the presence of a pro-domain; a
75 rate-limiting step in the folding process of subtilisin [9]. Remarkably, pro-domains of
76 numerous proteinases have been reported to assist as chaperones in both inter- and
77 intramolecular manner, following expression in trans- and cis- form, respectively [10-12]. An
78 analogous mode of action for such pro-domains, with no requirement for a covalent link
79 between propeptide and catalytic domain, has been discovered in other enzymes [13].
80 Indeed, both subtle and rather complex relationships between propeptide and catalytic
81 domain were found in subtilisin E, where an unaltered, mature polypeptide chain of subtilisin
82 E was shown to fold into a different conformation via a mutated intramolecular chaperone
83 and to show altered substrate specificity; a phenomenon termed `protein memory` [14].
84 Normally, such intramolecular chaperones precede catalytic domain from the N-terminus,
85 however, eukaryotic monozinc aminopeptidase A was found to recruit its C-terminal
86 propeptide for this role [15]. Such findings demonstrate the diverse and complex
87 relationships between the essential pro-domain and the cognate active conformation in the
88 proteogenesis of proteases.

89 The aminopeptidase from *Vibrio proteolyticus* (AAP) is a model bimetallohydrolase enzyme,
90 representing the M28 peptidase family (MH clan) whose extensive structural and functional
91 studies have provided an in-depth understanding of the mechanism of action and the substrate
92 preferences for these bi-metallic enzymes [16-25]. Furthermore, the role of the propeptide in
93 AAP and other homologous leucine aminopeptidases has been extensively studied *in vitro*

94 [26-28]. A number of studies have provided structural insights into AAP inhibition via
95 different synthetic compounds, acting as competitive inhibitors [18, 21, 22, 29]. However,
96 until now, no report exists to provide a detailed mechanistic insight for leucine
97 aminopeptidase inhibition by its natural competitive inhibitor – the N-terminal propeptide - at
98 the molecular level.

99 In this article, we present the crystal structures of recombinantly expressed LapA precursor
100 (AO-*pro*LapA), mature LapA (AO-*m*LapA) and mature form of the enzyme complexed with
101 reaction product l-leucine (AO-*m*LapA-Leu), all purified from *P. pastoris* culture
102 supernatant. To date, the exact mechanism of leucine aminopeptidase inhibition and the role
103 of an intramolecular chaperone (IMC) by the pro-domain has not been described in detail. To
104 the best of our knowledge, this is the first crystal structure of a leucine aminopeptidase
105 precursor, revealing detailed structural aspects of catalytic domain inhibition by the cognate
106 propeptide. This work shows that known synthetic aminopeptidase inhibitors and substrates
107 mimic key polar contacts between propeptide and the catalytic domain. These findings could
108 aid the future design of more effective inhibitors of bimetallic aminopeptidases and other
109 dizinc enzymes, sharing a similar reaction mechanism.

110 **Results & Discussion**

111 *Sequence comparison of Lap peptidases*

112 Extracellular aminopeptidases from the M28 family share a very similar sequence
113 composition of their open reading frames (ORF's). In general, a short secretion signal
114 sequence is preceded by a moderate length propeptide (removed in the maturation process),
115 which defines a central catalytic domain. It is convenient to compare their primary sequences
116 and their tertiary structure folds to establish conservation and evolutionary divergence at both
117 the sequence and structure level. Evolutionary relationships between Lap1 from *A. sojae* and

118 eukaryotic, as well as microbial homologues, were previously investigated [30]. In our study,
119 full ORF^s of several of these homologous fungal and microbial extracellular Lap enzymes
120 were aligned together with LapA from *A. oryzae* (AO-*pro*LapA) and Lap1 from *A. sojae*
121 (AS-*pro*LapA) (**Figure S1**). Despite AO-*pro*LapA sharing 97% sequence identity to AS-
122 *pro*LapA, these enzymes display remarkably distinct preferences for substrates [31].
123 Compared to highly conserved catalytic core residues, a varying degree of homology was
124 observed within the signal peptide and propeptide sequences. **Figure S1** shows that, of the 11
125 amino acids that differ in these two aminopeptidases, 5 reside within the propeptide region,
126 which is removed in the maturation process, and the other 6 lie within the mature
127 polypeptide. All of the different residues in AS-*pro*LapA, except Gly192, are distributed far
128 away from the catalytic centre, according to our model. Thus, the relationship between
129 substrate specificities and differences in amino acid sequence, among these peptidases, is
130 likely more subtle and translates either through a global network of intramolecular
131 interactions via small modifications in the catalytic domain, or an even more complex
132 relationship related to differences in the more variable propeptide sequence and its role as an
133 intramolecular chaperone.

134 LapA from *A. oryzae*, Lap1 from *A. sojae*, AAP from *Aeromonas proteolytica* and more
135 recently reported Lap enzymes from *Legionella pneumophila* [32] all belong to the M28
136 peptidase family; clan MH (MEROPS). AAP from *A. proteolytica* has been studied
137 extensively and has been a model enzyme for this family [16, 17]. Lap enzymes are typical
138 structural representatives of this family with two Zn(II) ions sequestered from the
139 surrounding environment and coordinated in the active site by 5 conserved residues in
140 sequence order His, Asp (coordinates both Zn(II) ions), Glu, Asp, Glu, His. Also, an
141 activated water molecule, associated with both metal ions, acts as a nucleophile during
142 catalysis. Additional Asp and Glu residues, considered to be essential for catalysis, reside in

143 close proximity within the His-Xaa-Asp and Glu-Glu motifs. Lap enzymes contain an archaic
144 alpha/beta hydrolase fold with a five-stranded beta sheet (1 strand antiparallel to the rest)
145 sandwiched between a layer of helices on each side. The active site is parallel to the end of
146 these beta strands.

147 The coordinated divalent zinc ions form a functional charge/dipole complex along with
148 conserved five amino acid ligands (AO-LapA numbering: H176, D195, E234, D261, H343).
149 Another conserved E233 residue, within the Glu-Glu motif, is supposed to assist in
150 deprotonation of the terminal catalytic water molecule and, subsequently, donating a proton
151 to newly formed amino-terminus, described as a rate-limiting step in the catalysis [23].
152 Several mutant forms of this residue render homologous AAP enzymes inactive [33, 34].
153 Also, a complementary second-shell hydrogen bond network was identified in AAP and
154 another homologous aminopeptidase from *Streptomyces griseus* (SGAP) [35]. We found that
155 the Zn-D261-S315-Q259-D316-S240 network, identified in the AAP structure, also was
156 conserved in our AO-LapA sequence and determined structure (**Figure 4, a**). Six residues
157 (M262, D338, Y312, C314, I342, F331) lining the hydrophobic specificity binding pocket of
158 AO-LapA (**Figure 2**) were also mostly conserved in homologous extracellular
159 aminopeptidases, including Lap1 from *A. sojae* (AS-proLap1) and AAP from *A. proteolytica*
160 (**Figure S1**). This analysis clearly suggest that AO-LapA, AAP and AS-LapA share a
161 conserved active site architecture, which in turn leads to highly conserved reaction
162 mechanism in these M28 aminopeptidases.

163 *LapA expression in recombinant hosts*

164 Coding regions of LapA precursor (AO-*proLapA*) and prodomain-deleted version (AO-
165 Δ *proLapA*) were codon-optimized for use by a *P. pastoris* host. Multiple gene dosage
166 transformants were obtained for both (pJ-*npro-LapA* and pJ- Δ *pro-LapA*) constructs.
167 However, no real-time qPCR was attempted to quantify the number of integrated gene copies,

168 in each case. Preliminary expression trials of the wild-type recombinant LapA with alpha
169 mating factor signal sequence and native LapA signal peptide resulted in slightly higher
170 secretion levels with the latter. Thus, it was decided to study further the expression of
171 recombinant LapA harbouring native signal peptide.

172 Determined molecular weight of recombinantly produced proenzyme was 39 kDa. Whilst the
173 mature enzyme showed the molecular weight of 32.5 kDa. The final molecular weight is
174 dependant on the extent of N-linked glycosylation at Asn87. The enzyme was not capable of
175 autoprocessing (autocatalytic cleavage of propeptide) following 72h incubation at ambient
176 temperatures in the purified form. The expression of precursor proteins is well established in
177 other metalloenzymes, such as subtilisin, thermolysin and homologous aminopeptidases from
178 *Aeromonas caviae* T-64 and *Vibrio proteolyticus* [27, 28, 36, 37]. Usually, these are
179 extracellularly secreted enzymes, where propeptide acts as a competitive inhibitor, including
180 subtilisin E [38], carboxypeptidase A [39], a metalloprotease from *Brevibacillus brevis* [40].
181 This could be an evolutionary adaptation to prevent non-specific intracellular proteolysis. The
182 catalytic nature of LapA can induce toxic effects to the host cell, therefore, most probably the
183 activation and processing of the LapA precursor in native *A. oryzae* occur following secretion
184 into the extracellular environment.

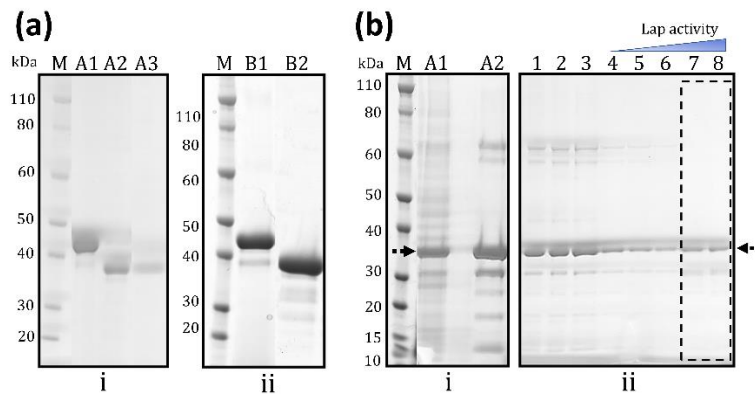
185 In the case of AO-mLapA and AO-*pro*LapA, expression levels reached approximately 0.3 g
186 per litre. SDS-PAGE analysis revealed significantly lower expression levels for AO-
187 *Δpro*LapA in *P. pastoris* supernatant (0.01 g/L) (**Figure 1**, a). We speculate that low
188 expression levels were observed, due to the absence of the prosequence in the pJ-*Δpro*-LapA
189 construct. Alternatively, it may be due to the integration of a lower copy number of LapA
190 genes. However, pJ-*Δpro*-LapA transformants were found to grow on YPD agar containing
191 2000 ug/ml Zeocin, which is very unlikely for the *P. pastoris* strain harbouring only a single
192 copy of the recombinant gene. The lack of propeptide in the AO-*Δpro*LapA expression

193 construct could have yielded misfolded protein with exposed hydrophobic patches,
194 associating with molecular chaperones, the mechanism by which unfolded proteins are
195 targeted for degradation within the ER [13, 41]. As a result, the observed expression levels
196 (**Figure 1**, a, i) were significantly lowered compared to AO-*proLapA*, which contained
197 propeptide in the expression cassette (**Figure 1**, a, i).

198 AO-*proLapA* and AO-*mLapA* recombinant proteins were obtained from the same expression
199 cassette (pJ-npro-LapA) and were a result of clonal variation within *P. pastoris*
200 transformants. Surprisingly, in one of the clones, unresolved processing of expressed
201 recombinant LapA precursor (AO-*proLapA*) occurred, yielding mature active AO-*mLapA*.
202 Most likely, cleavage of propeptide was a post-translational event since genomic PCR-based
203 sequencing within the coding region showed no deletion of propeptide (results not shown).
204 We propose that co-secreted non-specific proteolytic activity by an endogenous *P. pastoris*
205 peptidase was responsible for the processing of the LapA (AO-*proLapA*) precursor protein.
206 As a consequence, N-terminal sequencing of AO-*mLapA* and the observed electron density
207 (**Figure 2**, a) revealed three additional residues (A77, V78, T79) preceding the N-terminal
208 tyrosine, originally reported for AO-LapA [4]. The unobserved electron density for the C-
209 terminal prodomain residues, a result of mobility, likely is required for better accessibility for
210 activation by an endopeptidase involved in the maturation of AO-LapA precursor. Therefore,
211 an unexplained endopeptidase activity, likely present in the *P. pastoris* supernatant, was
212 different from that of native *A. oryzae*, which degrades the propeptide to N-terminal tyrosine
213 (Y80). This would seem to be the only viable explanation since, in the other clones, the vast
214 majority of recombinant protein was found in the form of the proenzyme (uncleaved
215 propeptide) in the culture supernatant.

216 As expected, *P. pastoris* supernatants with secreted AO-*m*LapA and AO-*pro*LapA contained
217 no other contaminant host proteins (**Figure 1**, a). This facilitated the subsequent purification
218 of these recombinant LapA (AO-*pro*LapA, AO-*Δpro*LapA, AO-*m*LapA) enzymes in the
219 absence of affinity tags. Importantly, repetitive AEX purification cycles were required to
220 liberate AO-*pro*LapA and AO-*m*LapA from a brown pigment existing in *P. pastoris*
221 supernatant. Elimination of these brown pigments proved very challenging, which was
222 deemed mandatory for crystallisation trials. Two brown pigments ($M_r < 2\text{kDa}$) were reported
223 previously to associate with other Lap peptidases and were briefly characterised by EPR to be
224 spectroscopically active and contain a Fe(III) ligand [42].

225 Over-expression of AO-*ref*LapA in *E. coli* was performed to test the feasibility of soluble
226 expression of the active catalytic domain (propeptide sequence omitted) of this eukaryotic
227 enzyme. AO-*ref*LapA protein was only recovered from inclusion bodies by urea renaturation
228 and subsequent 2-step purification (**Figure 1**, b). A dialysis step was required to liberate AO-
229 *ref*LapA from 200 mM imidazole, present in the IMAC-eluted fraction. It is worth noting that,
230 only a small portion of refolded AO-*ref*LapA was significantly active, following a size
231 exclusion chromatography (SEC) step (fractions 7 and 8, **Figure 1**, b, ii). The specific activity
232 of non-aggregated and refolded AO-*ref*LapA (fractions 7 - 8) reached 59.5 U/mg (**Table 1**).
233 These fractions were pooled and utilised in subsequent CD analysis (**Figure S2**). A large
234 population of AO-*ref*LapA separated as inactive, potentially aggregated protein (fractions 1 -
235 3, **Figure 1**, b, ii) using SEC. These high-MW aggregates were even visible under denaturing
236 SDS-PAGE and reducing buffer conditions. Attempts to isolate AO-LapA in soluble form in
237 *E. coli*, required an additional *in vitro* refolding step to restore some activity. However, the
238 catalytic activity was not fully recoverable, likely due to absence of propeptide and its
239 intramolecular chaperone effect (discussed later).



241 **Figure 1** Purification of Lap proteins. (a) – purification of AO-*mLapA*, AO-*proLapA* and AO-
 242 Δ *proLapA*: i) *P. pastoris* supernatants sampled (10 μ l) at 120 h, containing recombinant LapA
 243 proteins: A1 – AO-*proLapA*, A2 – AO-*mLapA*, A3 – AO- Δ *proLapA*; ii) purified from
 244 *P. pastoris* supernatant: B1 – AO-*proLapA*, B2 – AO-*mLapA*; (b) – purification of AO-
 245 *refLapA* (indicated by dotted arrows): i) initial IMAC purification step: A1 – resolubilized AO-
 246 *refLapA* inclusion bodies in 8M urea, A2 – imidazole eluted fraction from IMAC column; ii)
 247 subsequent SEC purification of IMAC-eluted fraction and dialysis-refolded protein, each lane
 248 corresponds to individual fractions. Active (under blue triangular activity bar) and the most
 249 active (dashed rectangle) fractions are indicated. M is molecular weight marker (Novex Sharp,
 250 Invitrogen, US).

251

252 The hydrolytic activity profiles of all the recombinant LapA forms were obtained against
 253 LPNA substrate under similar conditions (pH 7.2, 37 °C; **Table 1**), as previously reported in
 254 studies of homologous LapA proteins [30, 43]. The reaction and kinetic parameters of AO-
 255 *mLapA* were found to closely resemble wild-type VpAP (120 U/mg; k_{cat} (s^{-1}) = 82 ± 2 ; K_m
 256 (μ M) = 18 ± 1) [43]. Also, AO-*mLapA* appeared significantly more efficient than another
 257 close homologue LP-*proLapB* protein: k_{cat}/K_m (s^{-1}/mM^{-1}) = 637.75 of AO-*mLapA* versus
 258 k_{cat}/K_m (s^{-1}/mM^{-1}) = 0.345 of LP-*proLapB* for its substrate Lys-*pNA* [44]. AO-*mLapA*

259 appeared to be two orders of magnitude more efficient at hydrolysing its substrate, LPNA.

260 The observed catalytic efficiency for AO-*mLapA* represents a fully functional, activated

261 recombinant protein, possessing an appropriate three-dimensional fold (discussed in the

262 subsequent section).

263

		Specific activity		
(i)	Enzyme	(U/mg)	(ii)	Reaction kinetics of AO- <i>mLapA</i>
	AO- <i>proLapA</i>	0.8 ± 0.1	k_{cat} (s ⁻¹)	76.53 ± 0.5
	AO- <i>mLapA</i>	140.15 ± 4.8	K_{m} (μM)	120 ± 1.1
	AO- Δ <i>proLapA</i>	0.34 ± 0.1	$k_{\text{cat}}/K_{\text{m}}$ (s ⁻¹ /mM ⁻¹)	637.75 ± 2.5
	AO- <i>refLapA</i>	59.5 ± 1.1		

264 **Table 1** Specific activities of purified LapA proteins (i) and steady-state reaction kinetic

265 measurements (ii) for AO-*mLapA* protein. Activity is averaged from 3 independent

266 measurements with standard deviation determined.

267

268 ***Circular Dichroism (CD) of LapA proteins***

269 The isolated LapA proteins were analysed by far-UV CD to estimate their secondary

270 structure content and to study their folded states. The characteristic far-UV spectra of AO-

271 *refLapA*, AO-*mLapA* and AO- Δ *proLapA* proteins are shown in **Figure S2**.

272 The specific activity of AO-*refLapA* was 2-fold reduced compared to AO-*mLapA* and it was

273 predicted to exist in a molten globule state, according to CD analysis. This implies that

274 absence of propeptide, in the expression construct of AO-*refLapA*, gives rise to an

275 improperly folded protein, which was unable to regain its full native conformation under 20 h

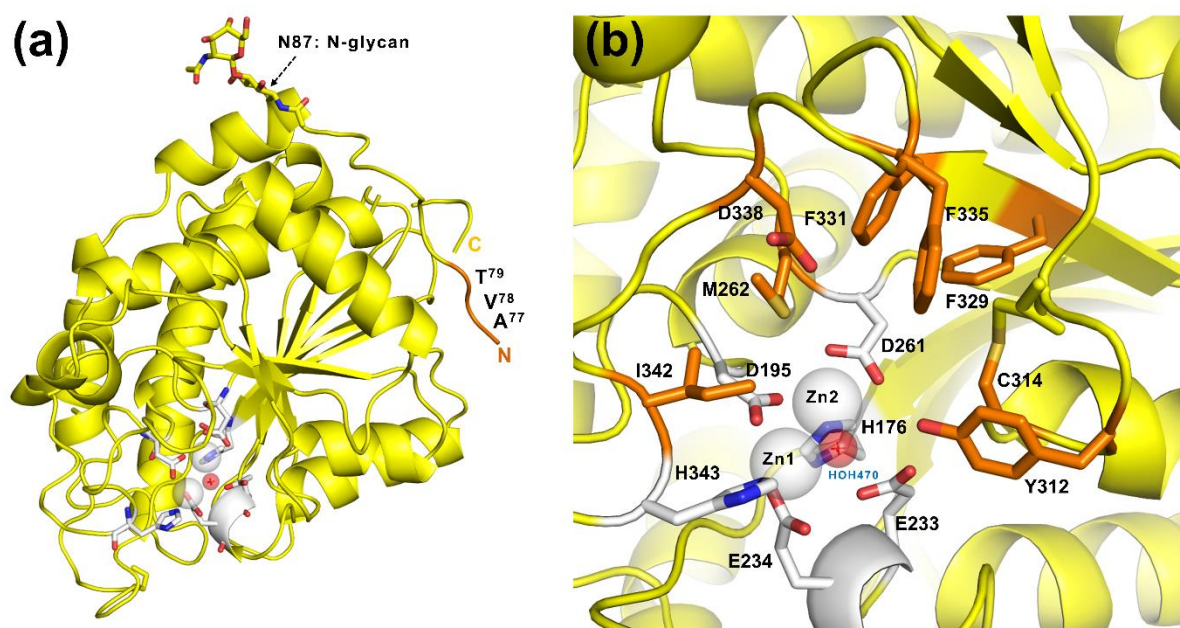
276 of refolding conditions. The lower content of secondary structure also was found in
277 recombinant refolded aminopeptidase from *V. proteolyticus* (AAP) compared to natively
278 expressed wild-type enzyme [45]. Finally, a spectral minimum at 200 nm and close-to-zero
279 ellipticity near 222 nm suggested a lack of secondary structure in the AO-*Apr*LapA protein
280 and a predominant pre-molten globule state, which explains its completely diminished
281 hydrolytic activity against Leu-*p*NA for this prodomain-truncated version of LapA protein
282 (**Table 1**). The differences in hydrolytic activity observed between recombinant LapA in *P.*
283 *pastoris* (AO-*Apr*LapA) and recombinant LapA in *E. coli* (AO-*ref*LapA) likely arise from
284 their different expression and isolation. AO-*ref*LapA was refolded *in vitro* from *E. coli*
285 inclusion bodies, using standard refolding conditions to favour folded, functional protein
286 [46]. However, AO-*Apr*LapA was naturally folded in the cytoplasm of *P. pastoris* and
287 secreted into the growth media, which could have led to misfolding (in the absence of its
288 prodomain), thus yielding less active protein. These observations demonstrate the negative
289 effect of the absence of the propeptide and signifies a potential role for the LapA propeptide
290 in assisting the mature domain to gain a fully folded, functional conformation essential for
291 maximal activity.

292

293 *Crystal structure of mature LapA (AO-mLapA)*

294 We determined a high-resolution crystal structure of the catalytic LapA domain to 1.97 Å.
295 We observed an additional three propeptide-derived amino acids (A77, A78, A79) at the N
296 terminus. Furthermore, additional electron density was observed for yeast-derived
297 glycosylation at residue N87 (**Figure 2, a**). The determined monomeric LapA structure (AO-
298 *m*LapA) forms a classical α/β globular domain. The hydrophobic core is comprised of a
299 twisted 8-stranded β -sheet, sandwiched between α -helices, representing a typical archaic
300 hydrolase fold. Secondary structure assignment, using the DSSP [47] server, showed that

301 45%, 16% and 39% of the residues are involved in α -helices, β -strands and coil structures,
302 respectively. An accessible active site pocket is located at the surface of the protein. The
303 catalytic binding pocket is formed by 6 conserved residues (H176, D195, D261, E233, E234,
304 H343), coordinating two Zn ions, embedded in the loop region close to the core parallel β
305 and β 5 sheets, and hydrophobic specificity pocket residues, mostly arranged at the C-terminal
306 end of the protein (**Figure 2**, b). The two Zn atoms are coordinated in a distorted tetrahedral
307 geometry with an average interatomic distance of 3.6 Å. We also identified a nucleophilic
308 water molecule bridging the two Zn atoms. Since both Zn ions significantly decrease the pK_a
309 of this water molecule [48], at the pH for optimal activity (8.0 – 9.0), it may exist as an OH^-
310 ion. However, under our crystallisation conditions for this structure (pH 5.0), it most likely
311 adopts an HOH molecule.



312

313 **Figure 2** Crystal structure of LapA catalytic domain (AO-*m*LapA) determined to 1.97 Å
314 resolution (a) and a close-up view of the active site and hydrophobic binding pockets (b).
315 Catalytic residues and coordinated Zn atoms are coloured in white; nucleophilic water,

316 HOH470, coordinated between the two Zn ions, indicated by red sphere; conserved
317 hydrophobic binding pocket residues are shown in orange sticks;

	AO- <i>pro</i> LapA	AO- <i>m</i> LapA	AO- <i>m</i> LapA-Leu
Data collection			
Beamline	DLS I02	DLS I02	DLS I04
Wavelength (Å)	0.9763	0.9763	0.9795
Space group	P 21 21 21	P 63 2 2	P 63 2 2
Unit-cell parameters			
<i>a</i> , <i>b</i> , <i>c</i> (Å)	43.43 94.39 99.11	153.92, 153.92, 88.64	154.1, 154.1, 87.83
<i>α</i> , <i>β</i> , <i>γ</i> (°)	90, 90, 90	90, 90, 120	90, 90, 120
Resolution range (Å)	42.61 - 1.61 (1.668 - 1.61)	73.81 - 1.97 (2.041 - 1.97)	73.37 - 2.48 (2.569 - 2.48)
No. of unique reflections	53338 (5269)	43992 (4297)	22302 (2195)
Redundancy	4.3 (4.2)	2.0 (2.0)	2.0 (2.0)
Completeness (%)	99.48 (99.55)	99.73 (99.33)	99.95 (99.95)
R _{sym} ^a or R _{merge} (%)	7.303 (89.15)	5.5 (61.81)	9.65 (48.29)
R _{meas}	0.08292	0.07729	0.1372
I/σ(I)	11.36 (1.59)	10.86 (1.21)	7.08 (1.55)
Refinement			
Resolution (Å)	42.61 - 1.61 (1.668 - 1.61)	73.81 - 1.97 (2.041 - 1.97)	73.37 - 2.48 (2.569 - 2.48)
No. reflections	53338 (5269)	43992 (4297)	22302 (2195)
R _{work} /R _{free} (%) ^b	15.27/17.39	16.45/20.36	15.69/21.50
No. atoms			
Protein	2698	2360	2390
Zn(II)	2	2	2
Chlorine	1	1	1
Water	482	462	360
Protein residues			
Protein	341	301	302
Average B-factors (Å ²)			
Protein	23.1	34.58	39.08
Zn(II)	18.9	30.38	44.45
l-leucine ligand	-	-	59.04
RMSD ^c			
bond lengths (Å)	0.007	0.008	0.007
bond angles (°)	1.250	0.95	0.94
Ramachandran Plot ^d			
Favored, Allowed, Disallowed (%)	98, 2.00, 0.00	98.33, 1.67, 0.00	97.66, 2.01, 0.33

The values in parentheses are for the highest resolution shell.

^a $R_{\text{sym}} = \frac{\sum_{\text{hkl}} \sum_i |I_i(\text{hkl}) - \langle I(\text{hkl}) \rangle|}{\sum_{\text{hkl}} \sum_i I_i(\text{hkl})}$, where $I_i(\text{hkl})$ and $\langle I(\text{hkl}) \rangle$ are the observed intensity and average intensity of multiple observations from symmetry-related reflections, respectively.

^b R_{work} was calculated with 95% of the data used for refinement, and R_{free} was calculated with 5% of the data excluded from refinement.

^c The RMSD stereochemistry value represents the deviation from ideal values.

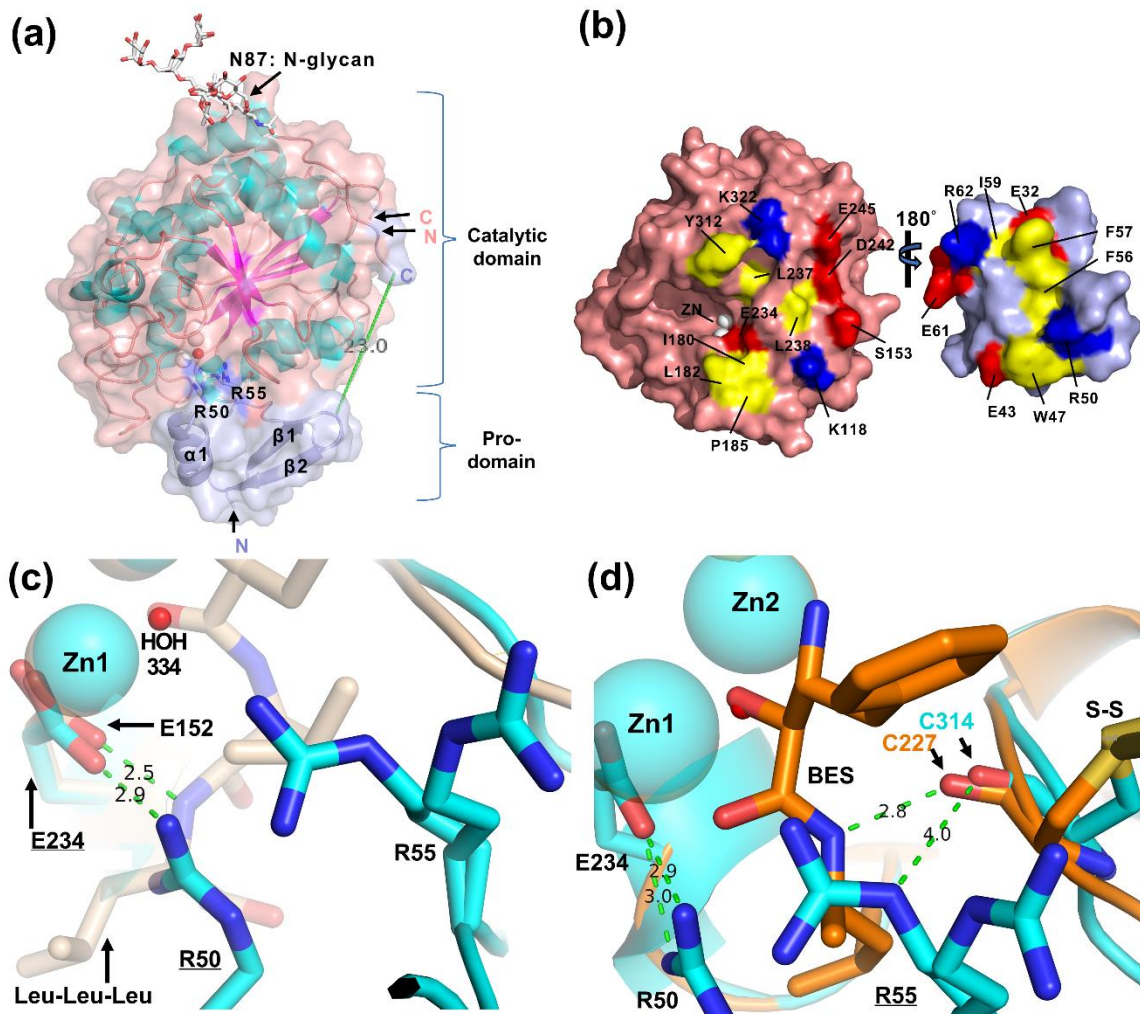
^d Ramachandran analysis was carried out using Molprobity.

319 *LapA precursor: propeptide-mediated inhibition of aminopeptidase domain*

320 The determined three-dimensional structure of LapA precursor (AO-*proLapA*) was refined to
321 1.61 Å resolution. All residues were well located in the electron density, with the exception
322 of residues 1 – 25 and 66 – 76 at N- and C-terminal region of the pro-domain, respectively,
323 due to inherent flexibility in these regions. The final model consisted of 341 residues, 482
324 water molecules, including the catalytic bridging water, a single chloride ion and an ethylene
325 glycol molecule (arising from cryo-protection).

326 From **Figure 3** (a), it is evident that the pro-domain extends from the junction with the
327 catalytic domain, follows alongside the catalytic core (residues 66 – 76 are missing, hence 23
328 Å gap) until it enters and occludes the catalytic cleft, using its 3-turn α -helix motif. The
329 overall structure of this separate domain is highly disordered and flexible: only 23% of total
330 residue content within the propeptide forms secondary structure. The middle part of the
331 propeptide sequence forms a 3-turn α -helix (residues 43-52) and a short 2-stranded β -sheet
332 (residues 29 - 31 and 39 - 41).

333



334

335 **Figure 3** Analysis of the crystal structure of LapA precursor (AO-*proLapA*), determined to
 336 1.6 Å resolution (PDBid: 6ZEP). (a) cartoon and surface representation of the final protein
 337 model: pro-domain is coloured in light blue, key arginines (R50, R55) are displayed as white
 338 sticks, catalytic Zn ions and coordinated water molecule are depicted as white and red
 339 spheres, respectively; a single glycosylated asparagine (N87) is indicated by stick
 340 representation of the attached sugar moieties. A missing, flexible region (residues 66 – 76),
 341 connecting the pro-domain and the catalytic domain, is indicated by a dashed green line along
 342 with a direct line measured distance in angstroms. (b) Contacts between the catalytic (left)
 343 and pro-domain (right). The pro-domain is rotated 180 degrees to expose the corresponding
 344 surface contacts. The domain interface is stabilised mainly by salt bridges (positively charged

345 residues – blue, negatively charged residues – red) and tight hydrophobic interactions
346 (yellow). Di-nuclear Zn site is shown as white spheres. Mechanism of propeptide-mediated
347 inhibition by the substrate (**c**) and inhibitor (**d**) mimicry. AO-*pro*LapA (in cyan) is
348 superimposed with AAP in complex with Leu-Leu-Leu substrate (PDBid: 2IQ6) (in wheat)
349 and inhibitor - bestatin (BES) (in orange) (PDBid: 1TXR). Key propeptide arginines R50 and
350 R55, catalytic glutamates E234 (AO-*pro*LapA) and E152 (AAP), equivalent disulphide
351 forming C314 (AO-*pro*LapA) and C227 (AAP) are labelled. Key electrostatic interactions are
352 measured in angstroms.

353 The propeptide buries 8.8% of mature domain solvent-accessible surface area (1,005 Å² of
354 11,474 Å²). This does not take into account the missing 66 – 76 residue region of the
355 propeptide. By corollary, the propeptide uses 29.7% of its surface area for the interface with
356 the mature domain (**Table S1**). The inter-domain network of interactions involves 37 and 21
357 (almost a half) of the residues for the catalytic and pro-domains, respectively. More
358 specifically, the inter-domain interface consists of 12 short-range (2.2 - 3.3 Å) H-bonds, 3
359 long-range (3.3 - 3.8 Å) H-bonds, 6 side chain-side chain salt bridges (< 3.3 Å), and at least
360 10 aliphatic side-chain residues within the propeptide that make tight hydrophobic contacts
361 with the mature domain (**Table S2**) (**Figure 3, b**).

362 Lastly, we identified Leu49 as a key propeptide fold stabilising residue. In the crystal
363 structure of LapA precursor, Leu49 was found to favourably interact with at least six adjacent
364 residues (**Figure S3**). These multiple hydrophobic interfaces, between the aliphatic side chain
365 of Leu49 and side chains of interconnecting residues, could be essential for stabilising the
366 overall fold of the pro-domain. Congruently, Leu70 in the LP-*pro*LapB structure was found
367 to be involved in multiple adjacent hydrophobic contacts alongside the Cys37 – Cys77
368 disulphide link [44]. We conclude that the strategically placed leucine residues significantly
369 contribute to stabilising the tertiary fold of the respective pro-domains, ensuring the correct

370 orientation of the $\alpha 1$ helix (**Figure 3**, a). The strategic orientation of the pro-domain helix
371 could be instrumental for steric occlusion of the active site cleft, thereby assisting in the
372 correct positioning of key inhibitory arginines (Arg50 and Arg55), discussed in the following
373 section.

374 *Mechanism of catalytic domain inhibition by LapA propeptide*

375 The crystal structure of LapA proenzyme enabled elucidation of the core inhibitory
376 interactions exerted by the propeptide domain, namely, two principal inhibitory arginines,
377 Arg50 and Arg55, penetrating the catalytic cleft to form specific interactions with highly
378 conserved residues, involved in peptide hydrolysis mechanism. Arg50, forms a tight 2.9 Å
379 hydrogen bond with OE1 of the catalytic Glu234 in the main chain (**Figure 3**, c). This
380 interaction directly mimics the analogous H-bond (2.5 Å) of Glu152 OE1 and the amide
381 group of P3` LLL ligand observed in the AAP-LLL structure (PDBid: 2iq6); one of three
382 essential H-bonds in forming the AAP-LLL pre-transition state complex [25]. The H-bond
383 angle between donor and receptor atoms of Glu152 and leucine substrate is 108° in the AAP-
384 LLL complex, while the analogous H-bond contact between Arg50 of the AO-*pro*LapA and
385 E234 is 147°, indicating a more favourable electrostatic interaction, suggesting a strong
386 inhibition mechanism by AO-*pro*LapA propeptide. The Arg50 – Glu234 interaction has a
387 significant effect on the coordination of this residue to the Zn1 atom. The Zn1 – O distance of
388 Glu234 OE1 (dangling oxygen) atom is 2.64 Å in the mature LapA structure, while in the
389 propeptide-inhibited structure this increases to 2.90 Å due to a strong electrostatic interaction
390 with both NH1 and NH2 nitrogens delivered by Arg50. Arg55 also contributes to the
391 inhibitory mechanism of LapA propeptide by providing a flexible terminal guanidinium
392 moiety, which (based on the electron density maps) we found to occupy three possible
393 orientations, supporting its inherent flexibility. Each of the three nitrogens in the guanidinium

394 moiety can potentially form favourable van der Waals contact with the carbonyl oxygen of
395 the adjacent Cys314 (**Figure 3**, d). This oxygen is involved in one of three key H-bond
396 contacts and the only H-bond present in the AAP complex with the LLL substrate (PDBid:
397 2iq6) and aminopeptidase bestatin (BES) inhibitor (PDBid: 1txr), respectively. We propose,
398 in a similar fashion, that the NE atom of the mobile Arg55 side chain is mimicking an
399 essential hydrogen bond contact between the backbone carbonyl oxygen of Cys227 and the
400 N1 atom of BES (2.8 Å). Also, the observed multiple orientations of Arg55 captured in our
401 electron density maps illustrates the dynamic behaviour of the side chain of this residue,
402 possibly distorting the di-nuclear Zn site by transiently interacting with the terminal nitrogens
403 on the guanidinium moiety. In this respect Arg50, likely together with Arg55, prevents
404 binding and initiation of substrate hydrolysis in *AO-proLapA*. This autoinhibitory
405 mechanism was not previously demonstrated in otherwise well studied M28 family of dizinc
406 aminopeptidases.

407 Importantly, the mechanism of Glu234 inhibition by recruitment of the Arg50 side chain in
408 the LapA pro-domain provides additional support to the proposed carboxylate-mediated
409 nucleophile delivery hypothesis presented by Kumar et. al (2007) [25]. While our data does
410 not directly indicate a role for Glu234 in catalysis, it does show that inhibition by the
411 propeptide is via blocking of one of the principal H-bonding sites for substrate binding. In
412 addition to sterically occluding the active site cleft, it is likely that the propeptide acts by
413 neutralising key residues, Glu234 and Tyr312, thereby preventing peptide hydrolysis. Until
414 more experimental data becomes available in the field, it can be confirmed that Zn1 ligand
415 and its role in the catalytic process is due to tuning the Lewis acidity of Zn1. The hydrogen
416 bond by Arg50 decreases the effective negative charge on the carboxylate group of Glu234
417 modulating the Zn1 Lewis acidity. The combination of steric hindrance of the active site
418 along with change in Lewis acidity of Zn1 ligand results in the loss of *AO-proLapA* activity.

419 This is well-established based on inhibited structures of AAP and other aminopeptidases
420 within this class.

421 *Pro-domain induced conformational changes in LapA precursor*

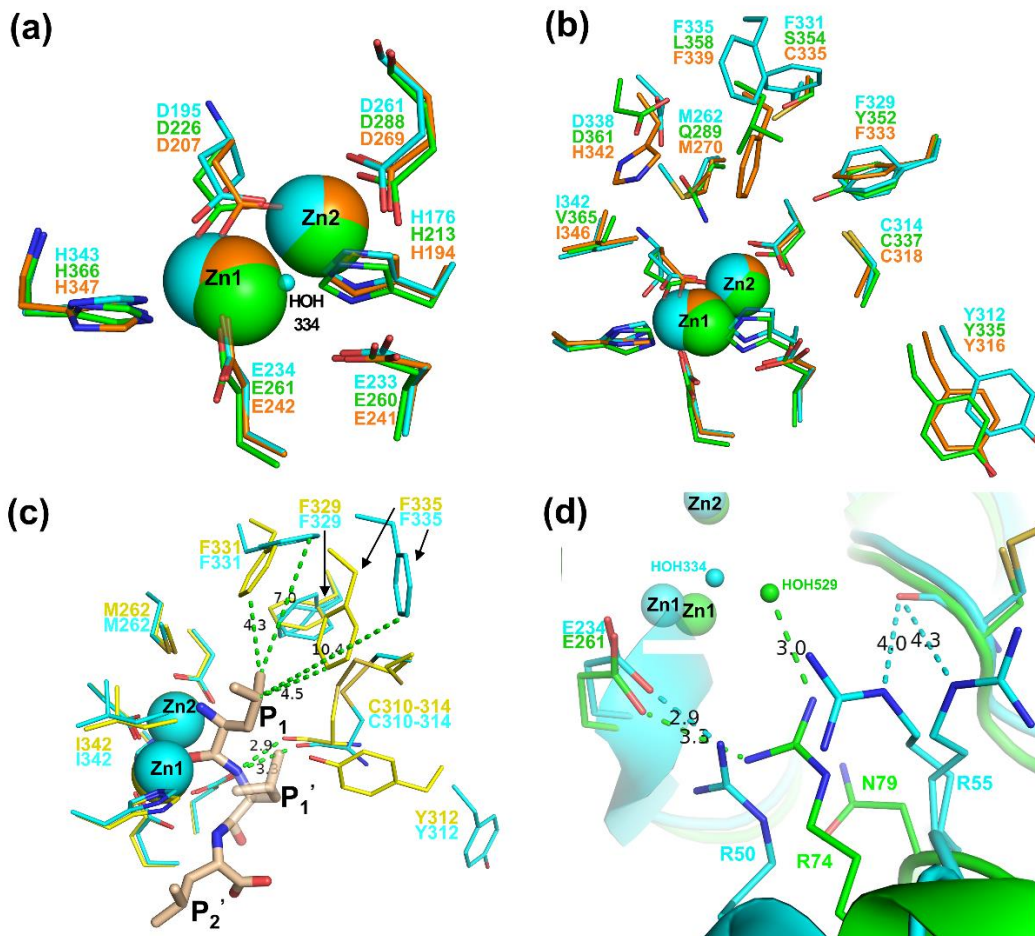
422 Given the high conservation in active site geometries for dimetallic zinc M28 peptidases, the
423 crystal structure of AAP in complex with the *bona fide* LLL (l-leucyl-l-leucyl-l-leucine)
424 substrate (PDBid: 2iq6) and synthetic inhibitor bestatin (PDBid: 1txr) provides direct
425 evaluation of propeptide-induced conformational changes within the substrate binding pocket
426 and corresponding HBP (hydrophobic binding pocket) residues (**Figure 3**, c and d; **Figure 4**,
427 c). LapA precursor was found to deviate from mature LapA only by 0.211 RMSD over an
428 equivalent range of residues (77 - 377). The presence of propeptide elicits several structural
429 rearrangements in the catalytic cleft of LapA precursor (**Figure 4**, c). Apart from the
430 conformational changes in the hydrophobic binding pocket (HBP) residues (discussed later),
431 the architecture of the active site is not altered significantly. However, very subtle changes in
432 the interatomic distances of the active site residues were detected. The distance between the
433 two catalytic Zn atoms is longer (3.6 Å) in the mature enzyme compared to LapA precursor
434 (3.4 Å). This stems from a minor change in Zn coordination distances with catalytic residue
435 ligands in the LapA precursor. Distinct loop movements in the residing regions of Cys310-
436 314 and Phe335 residues causes lengthening of the bond distance to the carbonyl oxygen of
437 Cys314, which forms direct contact with the amide nitrogen of the leucine substrate (P₁')
438 (**Figure 4**, c). This subtle (2.9 Å to 3.3 Å) H-bond lengthening is sufficient to weaken this
439 polar contact. Also, it is possible that the H-bond angle of this contact becomes less
440 favourable in the LapA precursor. Alteration of this contact might contribute to an impaired
441 ability to bind the substrate. Indeed, Cys314 has been identified as one of the key residues in
442 the hydrophobic substrate binding pocket in Lap1 from *A. sojae* [5]. Similarly, residue
443 Phe335 is directly involved in substrate binding in the mature enzyme, making a hydrophobic

444 contact ($\sim 4.5 \text{ \AA}$) with the sidechain of P₁ moiety (**Figure 4, c**). A significant movement of
445 the Phe335 side chain out of the active site (increasing the contact distance to 10.4 \AA), elicits
446 a less catalytically competent conformation in the LapA precursor.

447

448 Additionally, at least two more residues were significantly affected by the movement of the
449 Cys310-314s and Phe335s loops. An increase of $> 2 \text{ \AA}$ from the leucyl hydrophobic side
450 chain (P₁) of the bound substrate was observed for the aromatic ring of Phe331. Remarkably,
451 the side chain of Y312 is almost completely flipped by 180 degrees. A conserved residue,
452 Tyr225, in an equivalent location is found in the AAP protein (PDBid: 2iq6). In the initial
453 model of peptide hydrolysis, Tyr225 was proposed to interact with the N-terminus of the
454 incoming substrate [20]. However, this concept was later challenged by the AAP-bestatin and
455 AAP-LPA complexes, where it was concluded that Tyr225 may not be involved
456 mechanistically, but it provides yet another stabilising hydrophobic contact [22].
457 Additionally, the phenolic oxygen of Tyr225 shares a H-bond with BES, Tris, LeuP and IDH
458 ligands. In contrast, we demonstrate that the N-terminus of the P₁' leucyl moiety is too distant
459 to form a H-bond with the hydroxide of the Tyr312 side chain, but it could make a favourable
460 hydrophobic contact with the side chain of P₁' (**Figure 4, c**). In any scenario, this highlights
461 the importance of Tyr312 in stabilising the hydrophobic substrate, which is impaired in the
462 flipped orientation of Tyr312 observed in the LapA precursor and other orthologous members
463 of the M28 peptidase family (**Figure 4, b**). In fact, the flipped orientation of this residue is a

464 single common trait identified in the propeptide-inhibited structures of these homologues
 465 (Figure 4, b). Therefore, the catalytic importance of this residue cannot be overlooked.



466 **Figure 4** Structural comparison of LapA from *A. oryzae* to select orthologs from the M28
 467 family. LapA precursor is shown in cyan, mature LapA – in yellow, AAP-LLL complex – in
 468 wheat (PDBid: 2iq6), LapA from *L. pneumophila* (PDBid: 6esl) – in orange, LapB from *L.*
 469 *pneumophila* (PDBid: 5gne) – in green. (a) Superimposition of active site residues; (b)
 470 Superimposition of active site and hydrophobic binding pocket residues; (c) Structural
 471 alterations in LapA precursor compared to mature protein, involving the leucine tripeptide
 472 taken from the AAP-LLL crystal structure; (d) Direct comparison of the mechanisms of
 473 propeptide-mediated inhibition in LapA from *A. oryzae* versus LapB from *L. pneumophila*.
 474 Residue labels are coloured corresponding to their respective molecules.

475

476 ***Structural comparison of LapA from A. oryzae and known orthologs of the M28 family***

477 A number of crystal structures relating to family M28 aminopeptidases have been reported in
478 the literature [32, 44]. Pairwise sequence alignment between aminopeptidase LP-*proLapB*
479 from *L. pneumophila* (PDBid: 5gne), a homologous M28 peptidase, and full-length AO-
480 *proLapA* revealed only 31% identity and 48.5% similarity, and another *L. pneumophila*
481 aminopeptidase LP-*proLapA* showed only 26% identity and 41.5% similarity. However, the
482 tertiary fold similarity was strikingly high with AO-*proLapA* deviating by only 0.793 Å and
483 0.924 Å RMSD from LP-*proLapA* and LP-*proLapB*, respectively, over an equivalent range
484 of residues (26 – 377, AO-*proLapA* numbering). The active site geometry was found almost
485 identical in all three crystal structures, with highly conserved catalytic residues and dizinc
486 metal cofactors superimposing, almost exactly (**Figure 4**, a). Despite only low sequence
487 identity, these aminopeptidases displayed an identical conserved fold, which is in agreement
488 with proteins having greater conservation in tertiary structures and confirming their
489 classification as M28 family members.

490 Notable differences in the substrate binding pockets of these aminopeptidases are identified
491 (**Figure 4**, b). Conserved Phe329 and Phe331 are replaced by respective Tyr352 and Ser354
492 in LP-*proLapB*, which may be responsible for the preferential hydrolysis of positively
493 charged, hydrophilic substrates by this enzyme [49]. His342 and C335 substitutions in LP-
494 *proLapA* might be responsible for reported very broad specificity toward N-terminal
495 hydrolysis targets [32]. Interestingly, the mode of autoinhibition in LP-*proLapB* was quite
496 similar to AO-*proLapA*, albeit not identical. LP-*proLapB* only recruits a single Arg74 to
497 represent a substrate like-contact with Glu261 in a similar fashion to our observed
498 mechanism in AO-*proLapA* (**Figure 4**, d). Arg74 in LP-*proLapB* also makes significant
499 water-mediated contact with the active site Zn, not observed in our model of LapA precursor.
500 Quite the opposite role for propeptide was observed in the study of LP-*proLapA*

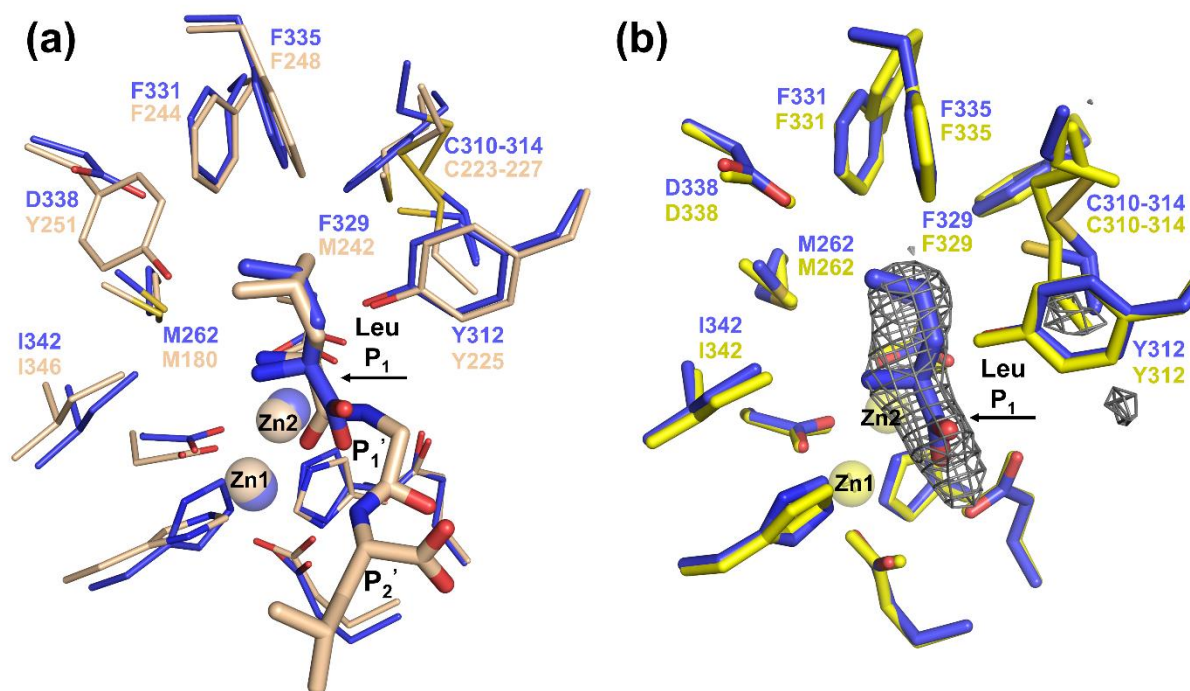
501 aminopeptidase, where no specific inhibitory-like interactions could be identified in the
502 crystal structure of its precursor. A weaker catalytic domain – propeptide interface was
503 exemplified by domain-swapping event captured in the dimer interface of the asymmetric
504 unit [32]. Also, enzymatic removal of pro-domain significantly diminished catalytic activity
505 in LP-*proLapA*. A directly opposite effect was observed in autoinhibitory AO-*proLapA* and
506 LP-*proLapB* peptidases, where the freed catalytic domain showed a substantial increase in a
507 specific activity.

508 *AO-LapA binding the reaction product – Leucine (AO-mLapA-Leu)*

509 Crystal structure of the recombinant mature LapA (AO-*mLapA*) in complex with a single
510 leucyl moiety was determined to 2.5 Å resolution. The crystallisation process involved briefly
511 soaking the previously formed AO-*mLapA* crystals in leucine tripeptide (Leu-Leu-Leu).
512 However, only a single leucine (P₁) could be reliably traced in the resulting electron density
513 map (**Figures 5**). Most likely, the enzyme exhibited hydrolytic activity in the crystalline
514 state, cleaving the scissile bond between P₁ and P₁' residues of the Leu-Leu-Leu substrate.

515 Several AAP crystal structures in complex with a natural substrate Leu-Leu-Leu tripeptide
516 [25] and substrate analogue 1-Butaneboronic acid [50] have been reported. The coordination
517 geometry of the leucyl moiety, in our AO-*mLapA*-Leu structure was almost identical to that
518 observed in the crystal structure of AAP-LLL for the P₁ moiety (PDBid: 2iq6) (**Figure 5, a**).
519 This observation reflects the conservation of the active site residues, substrate binding pocket
520 geometries and reaction mechanism for these homologous leucine aminopeptidases, which
521 display only 34% sequence identity.

522



523

524 **Figure 5** Comparison of the substrate binding pockets in AO-*mLapA*-Leu and AAP-LLL
 525 (PDBid: 2iq6) crystal structures. (a) Superimposition of active site residues, bound substrates
 526 and HBP residues. The isobutyl sidechain of the leucyl P₁' was omitted for clarity; (b)
 527 Superimposition of active site and HBP residues in resting (AO-*mLapA*) and Leu-bound
 528 (AO-*mLapA*-Leu) enzymes; Colour code: AO-*mLapA*-Leu – violet, AAP-LLL – wheat, AO-
 529 *mLapA* - yellow. The calculated interatomic distances between ligand and protein in the AO-
 530 *mLapA*-Leu structure are provided in **Table S3** and an Fo-Fc omit map for the Leu ligand is
 531 shown in grey mesh.

532

533 The distance between the two Zn atoms in the AO-*mLapA*-Leu complex is 3.3 Å, which is
 534 slightly less than that observed in the resting LapA molecule (3.6 Å). The isobutyl sidechain
 535 of the P₁ ligand interacts with an expansive, hydrophobic S₁ subsite, formed by the
 536 intervening sidechains of residues Tyr312, Cys314, Phe335, Phe329, Phe331, Met262 and
 537 Ile342, which all are within 5 Å of the ligand sidechain (**Figure 5**, b). Accommodation of the

538 leucine ligand elicited no major conformational changes of the key HBP residues, indicated
539 by an almost ideal superimposition with equivalent residues in resting AO-*mLapA* crystal
540 structure (RMSD 0.175 Å). The HBP residue sidechains ‘lock in’ the leucine moiety in the
541 active site pocket, which adopts a catalytically competent geometry that resembles the
542 unbound state. By contrast, we observed significant movements of key HBP residues in the
543 catalytically compromised state of autoinhibited enzyme (AO-*proLapA*) (**Figure 4**, c). Due
544 to the differences in ligand soaking times (into preformed crystals) compared to the published
545 AAP-LLL complex (PDBid: 2iq6), it appears that we likely trapped a post-catalysis state
546 showing only a single leucine bound to AO-*mLapA*.

547

548 **Conclusion**

549 In this work, the role of propeptide in the expression construct of LapA precursor was
550 investigated, using a *P. pastoris* recombinant expression platform. Due to the propeptide
551 deletion AO-*ΔproLapA*, recombinant LapA was secreted at significantly reduced levels
552 compared to full LapA precursor (AO-*proLapA*). Lack of the propeptide in AO-*ΔproLapA*
553 expression cassette could have yielded inappropriately folded protein with exposed
554 hydrophobic patches, associating with molecular chaperones, the mechanism by which
555 unfolded proteins are targeted for degradation within the ER of yeast [13, 41]. Hence, the
556 observed expression levels of AO-*ΔproLapA* protein were significantly reduced compared to
557 AO-*proLapA*, which contained propeptide in the expression construct, in turn escaping the
558 degradation mechanism. Using CD spectroscopy, AO-*ΔproLapA* was shown to exhibit a lack
559 of secondary structure, consequently, to exist in a predominantly pre-molten globule state,
560 while LapA was able to acquire a native fold in the presence of propeptide. This experiment
561 alone indicated a requirement of prosequence, acting as a chaperone in an intramolecular

562 manner. However, our crystal structures also reveal a plausible molecular mechanism of AO-
563 LapA catalytic domain inhibition by propeptide, further supporting a role for its N-terminal
564 domain as an intramolecular chaperone, in the process of maturation of AO-LapA zymogen.
565 We observed that the mature catalytic domain of AO-LapA is not able to achieve its native
566 conformation when produced in the absence of N-terminal prosegment. This observation is
567 reinforced by expression and refolding study of hexahistidine-tagged catalytic domain only
568 (AO-*ref*LapA) from *E. coli* inclusion bodies, revealing a limited active conformation.

569 This work also demonstrates that AO-LapA propeptide acts as an intramolecular chaperone
570 and is essential for the maturation of the catalytic domain when expressed in *cis*. We show
571 that AO-LapA prodomain may be able to function in an intermolecular manner and assist
572 with secretion and folding of the mature polypeptide when expressed in *trans*. This is in
573 agreement with other reported studies of prodomain expression in non-covalently linked state
574 (*trans*) for homologous and more distantly related peptidases. For example; expression of the
575 propeptide and mature domains, as separate polypeptides, resulted in the recovery of activity
576 for membrane Type 1-matrix metalloproteinase [51]; impeded secretion of the mature domain
577 of aspartic proteinase Sap1p from *C.albicans* in *P. pastoris* was restored upon co-expression
578 of the pro-polypeptide in *trans* [10]; and unlinked propeptide co-expression in *P. pastoris*
579 also was shown to rescue the appropriate secretion and activity levels of *Streptomyces*
580 *mobarraensis* Transglutaminase [13].

581 More generally, this work contributes to the knowledge of currently available crystal
582 structures of distantly related orthologous peptidases and offers an evolutionary and
583 biologically important model of propeptide-mediated inhibition for metalloenzymes of the
584 M28 family. Based on the available structural data from distant prokaryotic orthologs and our
585 high resolution Lap crystal structures presented herein, we also conclude that the catalytic
586 domain of AO-*pro*LapA is more specifically and strongly inhibited by its cognate propeptide,

587 recruiting long side chains of positively charged arginine residues. In the parent *A. oryzae*
588 eukaryotic cell this most likely evolved in order to prevent non-specific proteolysis of
589 essential amino peptides before secretion to the extracellular environment, whereas this may
590 not be so important in a less complex prokaryotic organism, such as *L. pneumophila*. Only
591 LP-*proLapB* showed autoinhibitory control over its catalytic domain, while removal of LP-
592 *proLapA* propeptide even reduced the catalytic rates and slightly modulated substrate
593 preference. Such detailed understanding of the autoinhibitory mechanism of cognate catalytic
594 domains by native propeptides could aid synthetic production of more effective inhibitors of
595 bimetallic aminopeptidases and other dizinc enzymes that share an analogous reaction
596 mechanism.

597

598

599 **Materials and Methods**

600 *Strains and plasmids*

601 *P. pastoris* BG10 strain was obtained from Biogrammatix Inc. (Carlsbad, CA, USA).
602 Secretary expression vector, pJ902, was provided by DNA 2.0 (USA). *E. coli* DH5 α (*fhuA2*
603 Δ (*argF-lacZ*)U169 *phoA glnV44 Φ 80 Δ (lacZ)M15 gyrA96 recA1 relA1 endA1 thi-1 hsdR17)*
604 cloning strain was purchased from New England Biolabs (NEB,UK).

605 All primers used in this study were obtained from Sigma (UK). ZeocinTM was purchased
606 from Invitrogen (USA). All other reagents were purchased from Sigma (UK) and were of
607 analytical grade.

608 *Construction of recombinant expression vectors and transformations in Pichia*
609 *pastoris*

610 Recombinant LapA open reading frames (Genebank accession: XP_001825745.1) were
611 codon-optimised and cloned into the pJ902 vector, by DNA 2.0, using the *EcoRI* and *NotI*
612 restriction sites. In this way, an expression construct harbouring the LapA native signal
613 peptide and propeptide sequences (pJ-npro-LapA) was obtained. A second expression
614 construct, containing a deletion of the LapA propeptide (pJ- Δ pro-LapA) was produced,
615 utilising the QuickChangeTM II site-directed mutagenesis kit from Stratagene (USA).
616 Deletion of the propeptide sequence was achieved by performing PCR with designed primers
617 1; 5'-GGACGCTATCTGGATAAGCTAATGCGCTTGCC-3' and 2; 5'-
618 GGCAAGCGCATTAGCTTATCCAGATAGCGTCC-3', using the pJ-npro-LapA construct
619 as a template.

620 Following *SacI*-mediated linearization and clean-up, recombinant plasmids were transformed
621 into an X33 expression strain by electroporation (a single 1500 V pulse in a 2 mm
622 electroporation cuvette). Immediately following electroporation, the cells were resuspended

623 in 0.5ml 1M sorbitol and 0.5ml YPD (1% yeast extract Y, 2% soy peptone P, 2% dextrose D)
624 and incubated for 2h at 30°C under gentle agitation. The revived cells were then plated onto
625 YPD agar (1% yeast extract, 2% soy peptone, 2% dextrose, 2% agar), containing either 100
626 µg/ml or 2000 µg/ml ZeocinTM and incubated at 30 °C for 2-4 days. The resulting *P. pastoris*
627 colonies were verified by PCR for appropriate genomic integration, using the method
628 previously described [52]. In each case, 10 transformants were screened picking the largest,
629 single colonies. Each single colony was patch-plated onto a separate YPD agar plate and
630 residual cells were re-suspended in 100µl lysis solution (200 mM lithium acetate, 1% SDS),
631 followed by incubation at 70 °C for 15 min. Following 96% ethanol precipitation, the DNA
632 pellet was re-suspended in 100 µl sterile water and 1µl (in each case) was used in each
633 subsequent genomic PCR. Clone ID (Lucigen, USA), PCR pre-mix and a pair of AOX
634 primers (AOX1-F; 5'-GACTGGTTCCAATTGACAAGC-3' and AOX1-R; 5'-
635 GCAAATGGCATTCTGACATCC-3') were used, under the following conditions: 1 cycle of
636 98 °C for 2 min, 30 cycles at 98 °C for 30 s, 56 °C for 30 s, 72 °C for 1 min, finishing with 72
637 °C for 5 min. The PCR products of predicted size were visualised on a 1% agarose gel.

638 ***Construction of recombinant expression vectors and transformation in E. coli***

639 Mature *A. oryzae* LapA polypeptide (Genebank accession: XP_001825745.1) was codon-
640 optimised and recombinantly cloned into a pET-21a expression vector (Eurofins, UK), using
641 *NdeI* and *BamHI* restriction sites. In this way, a pET-6xHis Δ proLapA expression construct
642 resulted, comprised of the T7 bacteriophage promoter, an N-terminal hexahistidine tag,
643 mature LapA polypeptide (minus propeptide) and an ampicillin resistance marker. This LapA
644 expression construct was transformed into BL21 (DE3) competent cells, according to the
645 manufacturer's instructions (New England Biolabs, US).

646 ***Over-expression of recombinant LapA in P. pastoris***

647 Recombinant LapA proteins were over-expressed in a *P. pastoris* X-33 strain (Mut⁺), under
648 control of the *P_{AOXI}* methanol inducible promoter. Shake flask expression trials were
649 conducted in BMGY (1% yeast extract, 2% soy peptone, 1% glycerol, 1.34% YNB, 4E-5%
650 biotin, 100mM potassium phosphate, pH 6.0) and BMMY (as for BMGY with 1% glycerol
651 replaced by 0.5% methanol). Genomic PCR-verified *P. pastoris* clones were inoculated into
652 50 ml BMGY medium in 250 ml baffled conical flasks and incubated in a shaker (250 rpm)
653 for 16 h at 28 °C. Once the OD₆₀₀ reached 2-8, an equivalent amount of cells (corresponding
654 to OD₆₀₀ of 1) were harvested and re-suspended in 100 ml of BMMY and shaken (250 rpm)
655 in 500 ml conical baffled flasks at 28 °C for 4-5 days. Every 24 h, the cultures were
656 supplemented with 0.5% final concentration of methanol to maintain induction and OD₆₀₀
657 cell densities were recorded. After 120 h of maintaining recombinant protein expression, the
658 cell cultures were harvested by centrifugation at 6000 x g for 15 min. The supernatant was
659 sampled and recombinant LapA protein detected by SDS-PAGE (NuPAGE® Novex® 4-12%
660 Bis-Tris gels).

661 ***Purification of recombinant LapA from P. pastoris supernatant***

662 Over-expressed AO-*pro*LapA, AO-*m*LapA, AO-*Δpro*LapA proteins were purified from *P.*
663 *pastoris* supernatant employing two different protocols: 1) crude *P. pastoris* supernatant,
664 containing recombinant LapA, was dialysed against 20 mM Tricine pH 8.0, 1 mM ZnCl₂ for
665 16 h at 4 °C, then filtered through a 0.22 μm steri-filter prior to loading onto a 5 mL
666 HiTrap™ Q HP anion exchange column (AEX), pre-equilibrated with 20 mM Tricine pH 8.0,
667 1 mM ZnCl₂. The column was washed (5 – 10 CV) with equilibration buffer until no trace of
668 protein appeared in the eluate. Recombinant LapA was eluted using an increasing gradient (0
669 - 1M) of NaCl (20 mM Tricine pH 8.0, 1 mM ZnCl₂, 1M NaCl). Active fractions were pooled
670 and concentrated, using ultrafiltration membranes (10 kDa MWCO). In each case, the

671 respective protein concentrate was loaded onto a HiLoad SuperdexTM 16/60 200pg (GE
672 Healthcare, UK) column, pre-equilibrated with 20 mM Tricine pH 8.0, 1 mM ZnCl₂.
673 Homogeneous recombinant LapA fractions were concentrated and stored at -20 °C for further
674 analysis; or 2) crude *P. pastoris* supernatant, containing the respective recombinant LapA
675 constructs, was saturated to 90% ammonium sulphate by adding hard salt, followed by
676 stirring for 1h at ambient temperature. LapA precipitant was pelleted by centrifugation at
677 16,000 *x g* for 20 minutes. The collected pellet was re-suspended in 20 mM Tricine pH 8.0, 1
678 mM ZnCl₂, followed by dialysis against the same buffer overnight at 4 °C. At this point, the
679 purification procedure was equivalent to 1), starting at the anion exchange chromatography
680 step. Recombinant proteins purified using protocols 1) and 2) were analysed on SDS-PAGE
681 for purity.

682 ***Over-expression of recombinant LapA in E. coli***

683 All preliminary recombinant LapA over-expression trials were carried out using 10 ml
684 cultures. A single BL21 (DE3) colony harbouring pET-6xHis Δ proLapA expression construct
685 was transferred to 2 mL LB broth and incubated at 37 °C (shaking at 220 rpm) overnight. 200
686 μ L of the overnight inoculum was transferred to 10 ml of fresh LB media. The optical density
687 (OD) at 600 nm was monitored regularly to reach a value between 0.5 and 1.0 absorbance
688 units, after which IPTG (1 mM final concentration) was added to induce protein expression
689 culture. The pre-induction sample was taken for further analysis on SDS-PAGE. The induced
690 cultures were then incubated for 16-20 h at either 37 °C or 20 °C. Following harvest at 16,000
691 *x g*, cells were lysed with BugBuster[®] Master Mix (Novagen) and soluble versus insoluble
692 protein fractions were analysed on SDS-PAGE.

693 ***Purification and refolding of AO-refLapA protein from E. coli inclusion bodies***

694 The pellet with inclusion bodies was re-solubilised in 8M urea buffer (50 mM Tricine pH 8.0,
695 500 mM NaCl, 8 M urea) gently agitating for 1 hour. The non-dissolved debris was separated

696 by centrifugation for 20 min at $16,000 \times g$. The resulting supernatant was loaded onto a
697 HisTrapTM FF 5 ml (GE Healthcare, UK) nickel immobilisation affinity column (IMAC), pre-
698 equilibrated with wash buffer (50 mM Tricine pH 8.0, 500 mM NaCl, 8 M urea) and re-
699 solubilised AO-*ref*LapA was eluted in 50 mM Tricine pH 8.0, 500 mM NaCl, 8 M urea and
700 200 mM imidazole. AO-*ref*LapA was allowed to slowly refold by reducing the concentration
701 of urea in the buffer: IMAC-eluted fraction was dialysed against refolding buffer (10 mM
702 Tricine pH 8.0, 1 mM ZnCl₂) for 20 h at 4 °C. The AO-*ref*LapA was further purified using a
703 HiLoad SuperdexTM 16/60 200pg (GE Healthcare, UK) gel filtration column pre-equilibrated
704 with 20 mM Tricine pH 8.0, 1 mM ZnCl₂. Sample collection (2 ml fractions) of fractions
705 exhibiting the highest specific activity were pooled and concentrated on Vivaspin 15R –
706 10,000 Dalton Centrifugal Filter Units (Sartorius, UK) containing the HydroSart®
707 membrane.

708 *Aminopeptidase assay*

709 LapA specific activity was determined spectrophotometrically, using a synthetic substrate l-
710 leucine-p-nitroanilide (LPNA) and monitoring the formation of the *p*-nitroanilide moiety
711 (*p*NA), as absorbance, at 405 nm ($\epsilon = 9.9 \text{ mmol}^{-1}\text{cm}^{-1}$) in a cuvette with a 1 cm path length.
712 Peptidase assays were performed on a CE1020 1000 Series spectrophotometer (Cecil
713 Instruments). One unit of LapA activity was defined to catalyse the hydrolysis of one
714 micromole of LPNA to l-leucine and *p*-nitroaniline, per minute at pH 7.2, 37 °C.

715 *Quantification of recombinant LapA*

716 LapA proteins were quantified either by Bradford assay (Bio-Rad, USA), using BSA as a
717 standard, or spectrophotometrically, employing a NanoDrop® ND-1000 (Thermo Scientific),
718 using the LapA absorbance extinction coefficient ($23,505 \text{ M}^{-1}\text{cm}^{-1}$). The concentration of
719 recombinant LapA in crude *P. pastoris* supernatant could only be determined by Bradford
720 assay due to impurities interfering with spectrophotometric measurements.

721 ***CD spectroscopy of recombinant LapA***

722 The circular dichroism spectra for all resultant proteins were recorded in the range 360 to 190
723 nm at 20 °C, using a Chirascan series 800 spectrophotometer. Measurements were taken
724 using a 1 nm step size in a 0.1 mm path length quartz cell. CD data were averaged from 5
725 independent scans for each sample. Samples of AO-*ref*LapA, AO-*m*LapA and AO- Δ *pro*LapA
726 proteins were analysed at 36 μ M, 21 μ M and 40 μ M concentrations, respectively, buffered in
727 20 mM HEPES pH 8.0.

728 ***Crystallisation and structure determination of recombinant LapA***

729 Crystallisation screening was carried out using HTP robotics at Oxford Protein Production
730 Facility (OPPF-UK) (96 well commercial sparse matrix screens, sitting-drop vapour diffusion
731 method) and crystallisation optimisation was carried out in the home laboratory using 24
732 well, hanging-drop vapour diffusion. AO-*pro*LapA, AO-*m*LapA recombinant proteins were
733 crystallised at concentrations of 13 mg/ml and 11 mg/ml, respectively. Both proteins were
734 buffer exchanged into 20 mM Tricine pH 8.0, 1 mM ZnCl₂ prior to crystallisation. AO-
735 *pro*LapA crystals with approximate dimensions 0.5 \times 0.04 \times 0.005 mm formed under F10
736 condition (0.1 M Bis-Tris, pH 5.5, 0.2 M NaCl, 25% PEG 3,350) in the Index HT™ screen
737 (Hampton Research, USA) over 3 days at 21 °C. AO-*m*LapA crystals were produced in 24-
738 well plate format at room temperature under previously identified F2 condition (0.1M Citrate,
739 pH 5.0, 3.2 M Ammonium sulphate) from the JCSGPlus HT™ screen (Molecular
740 Dimensions, UK).

741 Prior to data collection, crystals were cryo-protected by quick transfer through a mixture of
742 mother liquor and 20% ethylene glycol, followed by flash cooling to 100K in liquid nitrogen.
743 Diffraction data were collected at Diamond Light Source (UK), on beamlines I02 and I03.
744 The diffraction data were recorded, by fine slicing (0.1° degree oscillation), on a Pilatus 6M
745 detector. Indexing and integration were completed automatically by XDS [53] and xia2 [54].

746 All LapA structures were solved by maximum likelihood molecular replacement with
747 PHASER [55], using the coordinates of an established LapA homology model; LapA
748 homology model was generated using the IntFold2 server [56], which identified
749 aminopeptidase from *Vibrio sp.* (34% sequence identity) as a closely related structural
750 homologue (PDBid: 1RTQ), as the template. The resulting LapA models were manually built
751 and fitted to the electron density maps using COOT [57]. All structures were refined using
752 PHENIX [58], polder omit maps [59] were used to validate the presence of any potential
753 ligands. Structural comparisons and superimpositions were generated using the TM-align
754 server [60]. Final structural refinement statistics are provided in **Table 2**. Structural images
755 were prepared using PyMOL [The PyMOL Molecular Graphics System, Version 1.2r3pre,
756 Schrödinger, LLC].

757

758 **Accession numbers**

759 Structural data were deposited in the PDB database with the following accession codes: 6ZEP
760 (AO-*pro*LapA), 6ZEQ (AO-*m*LapA) and 6ZES (AO-*m*LapA-Leu).

761

762 **CRedit authorship contribution statement**

763 **Gediminas Baltulionis:** Conceptualization, Investigation, Methodology, Formal analysis,
764 Visualisation, Writing - original draft, Writing - review & editing. **Kimberly A. Watson:**
765 Funding acquisition, Conceptualization, Resources, Methodology, Formal analysis,
766 Visualisation, Supervision, Writing - review & editing, . **Mark Blight:** Conceptualization,
767 Resources, Methodology. **Aelig Robin:** Conceptualization, Resources, Methodology.
768 **Dimitris Charalampopoulos:** Funding acquisition, Conceptualisation, Resources,
769 Supervision, Writing - review & editing.

770

771 **Acknowledgments**

772 We thank Diamond Light Source, University of Reading and Biocatalysts Ltd. for access to
773 excellent facilities. This work was funded by a BBSRC CASE award BB/K012053/1 (to GB).

774

775 **Declarations of Interest:** None.

776

777

778

779 **References**

- 780 [1] Stressler T, Eisele T, Schlayer M, Lutz-Wahl S, Fischer L. Characterization of the
781 recombinant exopeptidases PepX and PepN from *Lactobacillus helveticus* ATCC 12046
782 important for food protein hydrolysis. *PLoS One*. 2013;8:e70055.
- 783 [2] Nampoothiri KM, Nagy V, Kovacs K, Szakacs G, Pandey A. l-leucine aminopeptidase
784 production by filamentous *Aspergillus* fungi. *Lett Appl Microbiol*. 2005;41:498-504.
- 785 [3] Lin LL, Hsu WH, Wu CP, Chi MC, Chou WM, Hu HY. A thermostable leucine
786 aminopeptidase from *Bacillus kaustophilus* CCRC 11223. *Extremophiles*. 2004;8:79-87.
- 787 [4] Matsushita-Morita M, Tada S, Suzuki S, Hattori R, Marui J, Furukawa I, et al.
788 Overexpression and Characterization of an Extracellular Leucine Aminopeptidase from
789 *Aspergillus oryzae*. *Curr Microbiol*. 2011;62:557-64.
- 790 [5] Huang WQ, Zhong LF, Meng ZZ, You ZJ, Li JZ, Luo XC. The Structure and Enzyme
791 Characteristics of a Recombinant Leucine Aminopeptidase rLap1 from *Aspergillus sojae* and
792 Its Application in Debittering. *Appl Biochem Biotechnol*. 2015;177:190-206.
- 793 [6] Lazure C. The peptidase zymogen proregions: nature's way of preventing undesired
794 activation and proteolysis. *Current pharmaceutical design*. 2002;8:511-31.
- 795 [7] Khan AR, Khazanovich-Bernstein N, Bergmann EM, James MN. Structural aspects of
796 activation pathways of aspartic protease zymogens and viral 3C protease precursors. *Proc Natl*
797 *Acad Sci U S A*. 1999;96:10968-75.
- 798 [8] Subbian E, Williamson, D. and Shinde, U. Protein Folding Mediated by an Intramolecular
799 Chaperone: Energy Landscape for Unimolecular Pro-Subtilisin E Maturation. *Advances in*
800 *Bioscience and Biotechnology*. 2015;6:73 - 88.
- 801 [9] Shinde U, Inouye M. Intramolecular chaperones: polypeptide extensions that modulate
802 protein folding. *Semin Cell Dev Biol*. 2000;11:35-44.
- 803 [10] Beggah S, Lechenne B, Reichard U, Foundling S, Monod M. Intra- and intermolecular
804 events direct the propeptide-mediated maturation of the *Candida albicans* secreted aspartic
805 proteinase Sap1p. *Microbiol-Uk*. 2000;146:2765-73.
- 806 [11] Tang B, Nirasawa S, Kitaoka M, Hayashi K. The role of the N-terminal propeptide of the
807 pro-aminopeptidase processing protease: refolding, processing, and enzyme inhibition.
808 *Biochem Bioph Res Co*. 2002;296:78-84.
- 809 [12] Safina D, Rafieva L, Demidyuk I, Gasanov E, Chestukhina G, Kostrov S. Involvement of
810 Propeptides in Formation of Catalytically Active Metalloproteinase from *Thermoactinomyces*
811 *sp*. *Protein Peptide Lett*. 2011;18:1119-25.
- 812 [13] Yurimoto H, Yamane M, Kikuchi Y, Matsui H, Kato N, Sakai Y. The pro-peptide of
813 *Streptomyces mobaraensis* transglutaminase functions in cis and in trans to mediate efficient
814 secretion of active enzyme from methylotrophic yeasts. *Biosci Biotechnol Biochem*.
815 2004;68:2058-69.
- 816 [14] Shinde UP, Liu JJ, Inouye M. Protein memory through altered folding mediated by
817 intramolecular chaperones. *Nature*. 1997;389:520-2.
- 818 [15] Rozenfeld R, Muller L, El Messari S, Llorens-Cortes C. The C-terminal domain of
819 aminopeptidase A is an intramolecular chaperone required for the correct folding, cell surface
820 expression, and activity of this monozinc aminopeptidase. *J Biol Chem*. 2004;279:43285-95.
- 821 [16] Schalk C, Remy JM, Chevrier B, Moras D, Tarnus C. Rapid purification of the *Aeromonas*
822 *proteolytica* aminopeptidase: crystallization and preliminary X-ray data. *Archives of*
823 *biochemistry and biophysics*. 1992;294:91-7.
- 824 [17] Chevrier B, Schalk C, D'Orchymont H, Rondeau JM, Moras D, Tarnus C. Crystal structure
825 of *Aeromonas proteolytica* aminopeptidase: a prototypical member of the co-catalytic zinc
826 enzyme family. *Structure*. 1994;2:283-91.

827 [18] Chevrier B, D'Orchymont H, Schalk C, Tarnus C, Moras D. The structure of the
828 *Aeromonas proteolytica* aminopeptidase complexed with a hydroxamate inhibitor.
829 Involvement in catalysis of Glu151 and two zinc ions of the co-catalytic unit. *European journal*
830 *of biochemistry / FEBS*. 1996;237:393-8.

831 [19] Bennett B, Holz RC. Spectroscopically distinct cobalt(II) sites in heterodimetallic forms
832 of the aminopeptidase from *Aeromonas proteolytica*: characterization of substrate binding.
833 *Biochemistry*. 1997;36:9837-46.

834 [20] Chen G, Edwards T, D'Souza V M, Holz RC. Mechanistic studies on the aminopeptidase
835 from *Aeromonas proteolytica*: a two-metal ion mechanism for peptide hydrolysis.
836 *Biochemistry*. 1997;36:4278-86.

837 [21] Stamper C, Bennett B, Edwards T, Holz RC, Ringe D, Petsko G. Inhibition of the
838 aminopeptidase from *Aeromonas proteolytica* by L-leucinephosphonic acid. Spectroscopic and
839 crystallographic characterization of the transition state of peptide hydrolysis. *Biochemistry*.
840 2001;40:7035-46.

841 [22] Stamper CC, Bienvenue DL, Bennett B, Ringe D, Petsko GA, Holz RC. Spectroscopic
842 and X-ray crystallographic characterization of bestatin bound to the aminopeptidase from
843 *Aeromonas (Vibrio) proteolytica*. *Biochemistry*. 2004;43:9620-8.

844 [23] Schurer G, Lanig H, Clark T. *Aeromonas proteolytica* aminopeptidase: an investigation
845 of the mode of action using a quantum mechanical/molecular mechanical approach.
846 *Biochemistry*. 2004;43:5414-27.

847 [24] Desmarais W, Bienvenue DL, Bzymek KP, Petsko GA, Ringe D, Holz RC. The high-
848 resolution structures of the neutral and the low pH crystals of aminopeptidase from *Aeromonas*
849 *proteolytica*. *J Biol Inorg Chem*. 2006;11:398-408.

850 [25] Kumar A, Periyannan GR, Narayanan B, Kittell AW, Kim J-J, Bennett B. Experimental
851 evidence for a metallohydrolase mechanism in which the nucleophile is not delivered by a
852 metal ion: EPR spectrokinetic and structural studies of aminopeptidase from *Vibrio*
853 *proteolyticus*. *Biochem J*. 2007;403:527-36.

854 [26] Zhang ZZ, Nirasawa S, Nakajima Y, Yoshida M, Hayashi K. Function of the N-terminal
855 propeptide of an aminopeptidase from *Vibrio proteolyticus*. *Biochem J*. 2000;350 Pt 3:671-6.

856 [27] Bzymek KP, D'Souza VM, Chen G, Campbell H, Mitchell A, Holz RC. Function of the
857 signal peptide and N- and C-terminal propeptides in the leucine aminopeptidase from
858 *Aeromonas proteolytica*. *Protein expression and purification*. 2004;37:294-305.

859 [28] Nirasawa S, Nakajima Y, Zhang ZZ, Yoshida M, Hayashi K. Intramolecular chaperone
860 and inhibitor activities of a propeptide from a bacterial zinc aminopeptidase. *Biochem J*.
861 1999;341 (Pt 1):25-31.

862 [29] Hanaya K, Suetsugu M, Saijo S, Yamato I, Aoki S. Potent inhibition of dinuclear zinc(II)
863 peptidase, an aminopeptidase from *Aeromonas proteolytica*, by 8-quinolinol derivatives:
864 inhibitor design based on Zn²⁺ fluorophores, kinetic, and X-ray crystallographic study. *J Biol*
865 *Inorg Chem*. 2012;17:517-29.

866 [30] Chien HC, Lin LL, Chao SH, Chen CC, Wang WC, Shaw CY, et al. Purification,
867 characterization, and genetic analysis of a leucine aminopeptidase from *Aspergillus sojae*.
868 *Biochim Biophys Acta*. 2002;1576:119-26.

869 [31] !!! INVALID CITATION !!! [4, 5].

870 [32] White RC, Gunderson FF, Tyson JY, Richardson KH, Portlock TJ, Garnett JA, et al. Type
871 II Secretion-Dependent Aminopeptidase LapA and Acyltransferase PlaC Are Redundant for
872 Nutrient Acquisition during *Legionella pneumophila* Intracellular Infection of Amoebas.
873 *MBio*. 2018;9.

874 [33] Bzymek KP, Holz RC. The catalytic role of glutamate 151 in the leucine aminopeptidase
875 from *Aeromonas proteolytica*. *J Biol Chem*. 2004;279:31018-25.

876 [34] Bzymek KP, Swierczek SI, Bennett B, Holz RC. Spectroscopic and thermodynamic
877 characterization of the E151D and E151A altered leucine aminopeptidases from *Aeromonas*
878 *proteolytica*. *Inorg Chem*. 2005;44:8574-80.

879 [35] Gilboa R, Greenblatt HM, Perach M, Spungin-Bialik A, Lessel U, Wohlfahrt G, et al.
880 Interactions of *Streptomyces griseus* aminopeptidase with a methionine product analogue: a
881 structural study at 1.53 Å resolution. *Acta Crystallogr D Biol Crystallogr*. 2000;56:551-8.

882 [36] Ikemura H, Takagi H, Inouye M. REQUIREMENT OF PRO-SEQUENCE FOR THE
883 PRODUCTION OF ACTIVE SUBTILISIN-E IN *ESCHERICHIA-COLI*. *J Biol Chem*.
884 1987;262:7859-64.

885 [37] Gao X, Wang J, Yu DQ, Bian F, Xie BB, Chen XL, et al. Structural basis for the
886 autoprocessing of zinc metalloproteases in the thermolysin family. *Proc Natl Acad Sci U S A*.
887 2010;107:17569-74.

888 [38] Hu Z, Haghjoo K, Jordan F. Further evidence for the structure of the subtilisin propeptide
889 and for its interactions with mature subtilisin. *J Biol Chem*. 1996;271:3375-84.

890 [39] Segundo BS, Martinez MC, Vilanova M, Cuchillo CM, Aviles FX. The severed activation
891 segment of porcine pancreatic procarboxypeptidase A is a powerful inhibitor of the active
892 enzyme. Isolation and characterisation of the activation peptide. *Biochimica et biophysica acta*.
893 1982;707:74-80.

894 [40] Serkina AV, Gorozhankina TF, Shevelev AB, Chestukhina GG. Propeptide of the
895 metalloprotease of *Brevibacillus brevis* 7882 is a strong inhibitor of the mature enzyme. *FEBS*
896 *Lett*. 1999;456:215-9.

897 [41] McIver KS, Kessler E, Olson JC, Ohman DE. The elastase propeptide functions as an
898 intramolecular chaperone required for elastase activity and secretion in *Pseudomonas*
899 *aeruginosa*. *Mol Microbiol*. 1995;18:877-89.

900 [42] !!! INVALID CITATION !!! [16, 19, 41, 42].

901 [43] Hartley M, Yong W, Bennett B. Heterologous expression and purification of *Vibrio*
902 *proteolyticus* (*Aeromonas proteolytica*) aminopeptidase: a rapid protocol. *Protein expression*
903 *and purification*. 2009;66:91-101.

904 [44] Zhang N, Yin S, Zhang W, Gong X, Zhang N, Fang K, et al. Crystal Structure and
905 Biochemical Characterization of an Aminopeptidase LapB from *Legionella pneumophila*. *J*
906 *Agric Food Chem*. 2017;65:7569-78.

907 [45] Hernandez-Moreno AV, Villasenor F, Medina-Rivero E, Perez NO, Flores-Ortiz LF,
908 Saab-Rincon G, et al. Kinetics and conformational stability studies of recombinant leucine
909 aminopeptidase. *International journal of biological macromolecules*. 2014;64:306-12.

910 [46] Singh SM, Panda AK. Solubilization and refolding of bacterial inclusion body proteins. *J*
911 *Biosci Bioeng*. 2005;99:303-10.

912 [47] Kabsch W, Sander C. Dictionary of protein secondary structure: pattern recognition of
913 hydrogen-bonded and geometrical features. *Biopolymers*. 1983;22:2577-637.

914 [48] Desmarais WT, Bienvenue DL, Bzymek KP, Holz RC, Petsko GA, Ringe D. The 1.20 Å
915 resolution crystal structure of the aminopeptidase from *Aeromonas proteolytica* complexed
916 with tris: a tale of buffer inhibition. *Structure*. 2002;10:1063-72.

917 [49] Rossier O, Dao J, Cianciotto NP. The type II secretion system of *Legionella pneumophila*
918 elaborates two aminopeptidases, as well as a metalloprotease that contributes to differential
919 infection among protozoan hosts. *Appl Environ Microbiol*. 2008;74:753-61.

920 [50] De Paola CC, Bennett B, Holz RC, Ringe D, Petsko GA. 1-Butaneboronic acid binding to
921 *Aeromonas proteolytica* aminopeptidase: a case of arrested development. *Biochemistry*.
922 1999;38:9048-53.

923 [51] Cao J, Hymowitz M, Conner C, Bahou WF, Zucker S. The propeptide domain of
924 membrane type 1-matrix metalloproteinase acts as an intramolecular chaperone when
925 expressed in trans with the mature sequence in COS-1 cells. *J Biol Chem*. 2000;275:29648-53.

- 926 [52] Looke M, Kristjuhan K, Kristjuhan A. Extraction of genomic DNA from yeasts for PCR-
927 based applications. *Biotechniques*. 2011;50:325-8.
- 928 [53] Kabsch W. Xds. *Acta Crystallogr D Biol Crystallogr*. 2010;66:125-32.
- 929 [54] Winter G, Lobley CM, Prince SM. Decision making in xia2. *Acta Crystallogr D Biol*
930 *Crystallogr*. 2013;69:1260-73.
- 931 [55] McCoy AJ, Grosse-Kunstleve RW, Storoni LC, Read RJ. Likelihood-enhanced fast
932 translation functions. *Acta Crystallogr D Biol Crystallogr*. 2005;61:458-64.
- 933 [56] Roche DB, Buenavista MT, Tetchner SJ, McGuffin LJ. The IntFOLD server: an integrated
934 web resource for protein fold recognition, 3D model quality assessment, intrinsic disorder
935 prediction, domain prediction and ligand binding site prediction. *Nucleic acids research*.
936 2011;39:W171-6.
- 937 [57] Emsley P, Cowtan K. Coot: model-building tools for molecular graphics. *Acta Crystallogr*
938 *D Biol Crystallogr*. 2004;60:2126-32.
- 939 [58] Adams PD, Afonine PV, Bunkoczi G, Chen VB, Davis IW, Echols N, et al. PHENIX: a
940 comprehensive Python-based system for macromolecular structure solution. *Acta Crystallogr*
941 *D Biol Crystallogr*. 2010;66:213-21.
- 942 [59] Liebschner D, Afonine PV, Moriarty NW, Poon BK, Sobolev OV, Terwilliger TC, et al.
943 Polder maps: improving OMIT maps by excluding bulk solvent. *Acta Crystallogr D Struct*
944 *Biol*. 2017;73:148-57.
- 945 [60] Zhang Y, Skolnick J. TM-align: a protein structure alignment algorithm based on the TM-
946 score. *Nucleic acids research*. 2005;33:2302-9.

947